

Structural Basis of a Rationally Rewired Protein-Protein Interface Critical to Bacterial Signaling

Anna I. Podgoraia,^{1,2,7} Patricia Casino,^{4,5,7} Alberto Marina,^{4,6,*} and Michael T. Laub^{2,3,*}

¹Computational and Systems Biology Initiative

²Department of Biology

³Howard Hughes Medical Institute

Massachusetts Institute of Technology, Cambridge, MA 02139, USA

⁴Instituto de Biomedicina de Valencia, Consejo Superior de Investigaciones Científicas (CSIC), 46010 Valencia, Spain

⁵Instituto de Biología Molecular de Barcelona, Consejo Superior de Investigaciones Científicas (CSIC), 08028 Barcelona, Spain

⁶CIBER de Enfermedades Raras (CIBERER), ISCIII, 46010 Valencia, Spain

⁷These authors contributed equally to this work and are co-first authors

*Correspondence: amarina@ibv.csic.es (A.M.), laub@mit.edu (M.T.L.)

<http://dx.doi.org/10.1016/j.str.2013.07.005>

SUMMARY

Two-component signal transduction systems typically involve a sensor histidine kinase that specifically phosphorylates a single, cognate response regulator. This protein-protein interaction relies on molecular recognition via a small set of residues in each protein. To better understand how these residues determine the specificity of kinase-substrate interactions, we rationally rewired the interaction interface of a *Thermotoga maritima* two-component system, HK853-RR468, to match that found in a different two-component system, *Escherichia coli* PhoR-PhoB. The rewired proteins interacted robustly with each other, but no longer interacted with the parent proteins. Analysis of the crystal structures of the wild-type and mutant protein complexes and a systematic mutagenesis study reveal how individual mutations contribute to the rewiring of interaction specificity. Our approach and conclusions have implications for studies of other protein-protein interactions and protein evolution and for the design of novel protein interfaces.

INTRODUCTION

Interacting protein partners must recognize each other while avoiding unproductive interactions within the crowded milieu of the cell. The residues important for a given protein-protein interface must therefore both promote interaction between cognate proteins and prevent, or at least minimize, all possible noncognate pairings. The challenge of maintaining specificity is particularly acute for proteins that belong to large paralogous protein families, which often share significant similarity to one another at the sequence and structural levels (Gao and Stock, 2009; Keskin et al., 2008).

In bacteria, two-component signal transduction proteins are a prevalent mechanism for sensing and responding to the environment. These signaling pathways rely on a sensor histidine kinase that can autophosphorylate and transfer its phosphoryl group to a cognate response regulator (Stock et al., 2000). Many histidine kinases are bifunctional and can directly dephosphorylate their cognate response regulators (Huynh and Stewart, 2011; Igo et al., 1989). Histidine kinases and response regulators are two of the largest protein families in bacteria, with most organisms encoding tens to hundreds of each type of protein (Alm et al., 2006; Galperin, 2005). However, most histidine kinases phosphorylate only a single cognate response regulator and there is very little crosstalk observed between noncognate partners (Capra et al., 2012; Laub and Goulian, 2007). Systematic studies of phosphotransfer have demonstrated that histidine kinases typically exhibit a strong kinetic preference for their cognate response regulators in vitro, suggesting that the interaction specificity of these signaling pathways is driven largely by molecular recognition rather than the cellular context (Fisher et al., 1996; Skerker et al., 2005).

Previous studies have demonstrated that interaction specificity is dictated by a small subset of residues on each protein (Capra et al., 2010; Skerker et al., 2008). These studies relied on the identification of coevolving amino acids in large multiple sequence alignments of cognate kinase-regulator pairs from a diverse range of bacterial species (Codoñer and Fares, 2008). The importance of these residues was validated through the rational rewiring of phosphotransfer specificity. Substituting the specificity residues in the *Escherichia coli* histidine kinase EnvZ with those found in other kinases was sufficient to drive phosphotransfer toward previously noncognate response regulators. A similar rewiring of the response regulator OmpR allowed it to receive phosphoryl groups from other histidine kinases. These coevolving specificity residues were confirmed as critical to molecular recognition when the first structure of a histidine kinase in complex with its cognate response regulator was solved (Casino et al., 2009, 2010). The complex of *Thermotoga maritima* kinase HK853 bound to a phosphorylated form of RR468 demonstrated that the primary basis of interaction involves the docking of helix $\alpha 1$ ($\alpha 1$) in the response regulator with both helices of the

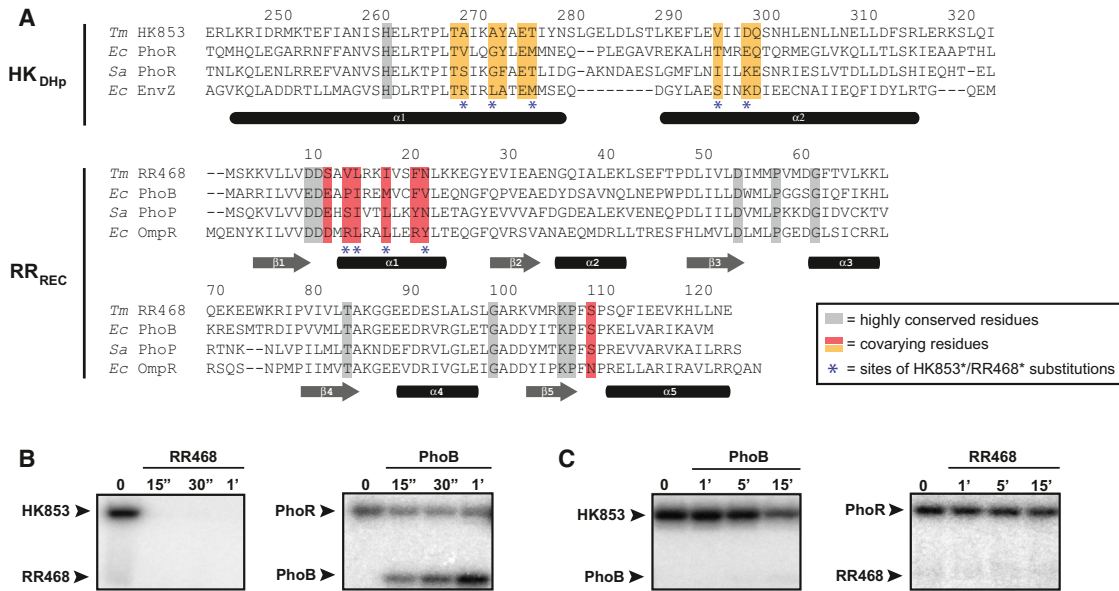


Figure 1. Specificity Residues in Two-Component Signaling Proteins

(A) Multiple sequence alignment of histidine kinases (DHP domain only) and response regulator (receiver domain only), with specificity residues and highly conserved residues highlighted. Species abbreviations: *Ec*, *Escherichia coli*; *Sa*, *Staphylococcus aureus*; *Tm*, *Thermotoga maritima*. Interacting partners are arranged in the same order in both HK and RR alignments. Sequences are numbered according to the *Tm* proteins, with the last digit of each number positioned above the relevant amino acid residue.

(B and C) HK853 and PhoR phosphotransfer specificity. Each histidine kinase construct was autophosphorylated with [³²P-γ]ATP and then incubated with the response regulator indicated at room temperature. Samples were taken at the time points indicated and phosphotransfer assessed by SDS-PAGE and phosphorimaging. Arrowheads indicate the position of autophosphorylated kinase or phosphorylated response regulator.

See also Figure S1.

dimerization and histidine phosphotransfer (DHP) domain in the kinase. Nearly all of the specificity residues identified via coevolution studies are found within these helices (Figure 1A).

Although two-component proteins have been successfully rewired, it remains unclear how a newly introduced set of specificity residues is accommodated at the molecular interface formed by a histidine kinase and a response regulator. How do individual residues contribute to the rewired specificity of a complex? How do the new residues pack together? Do changes at the interface affect other, distal regions of the proteins? To tackle these questions, we rationally rewired the interaction interface of *T. maritima* proteins HK853 and RR468 to harbor the specificity-determining residues of an unrelated two-component pathway, *E. coli* PhoR and PhoB. We solved crystal structures of complexes formed by the rewired proteins, as well as the structures of the rewired HK853 and RR468 alone. Comparison of these structures with the native HK853-RR468 complex, along with a systematic mutational analysis of the interface, helps reveal the structural basis of specificity in two-component signaling proteins. More generally, they provide insight into the rules of molecular recognition and coevolution in protein-protein interfaces.

RESULTS

HK853-RR468 and PhoR-PhoB Have Different Phosphotransfer Specificities

To investigate the structural consequences of rewiring a kinase-substrate interface, we rationally mutated the specificity resi-

dues of the *T. maritima* two-component pathway HK853-RR468 to match those of another two-component system. Previous work has shown that unlike the model kinase EnvZ, the HK853 homodimer autophosphorylates in *cis*, such that the histidine on a given chain is autophosphorylated by the ATP-binding domain of the same chain (Casino et al., 2009). We therefore aimed to reprogram the specificity of the HK853-RR468 system to match that of another system in which the kinase autophosphorylates in *cis*, the *E. coli* system PhoR-PhoB (Ashenberg et al., 2013; Casino et al., 2009). HK853 and *E. coli* PhoR are ~32% identical at the amino acid level across their DHP and catalytic and ATP binding (CA) domains and share four identities at the nine specificity positions. RR468 and *E. coli* PhoB are ~38% identical across their receiver domains and share two identities at the seven specificity positions (Figure 1A; Figure S1A available online).

To confirm that the different specificity residues in HK853-RR468 and PhoR-PhoB yield different phosphotransfer specificities, we purified His₆-tagged versions of each protein. For HK853 and PhoR, we truncated the transmembrane domains, purifying only the soluble, cytoplasmic portions of each kinase (see Experimental Procedures). RR468 has only a receiver domain, whereas PhoB has a receiver domain and a DNA-binding domain; we purified the receiver domain portion of each regulator. We first autophosphorylated each kinase in the presence of [γ-³²P]ATP and then added cognate substrates to examine phosphotransfer. At room temperature, HK853 rapidly phosphorylated RR468 (Figure 1B). Because HK853 is

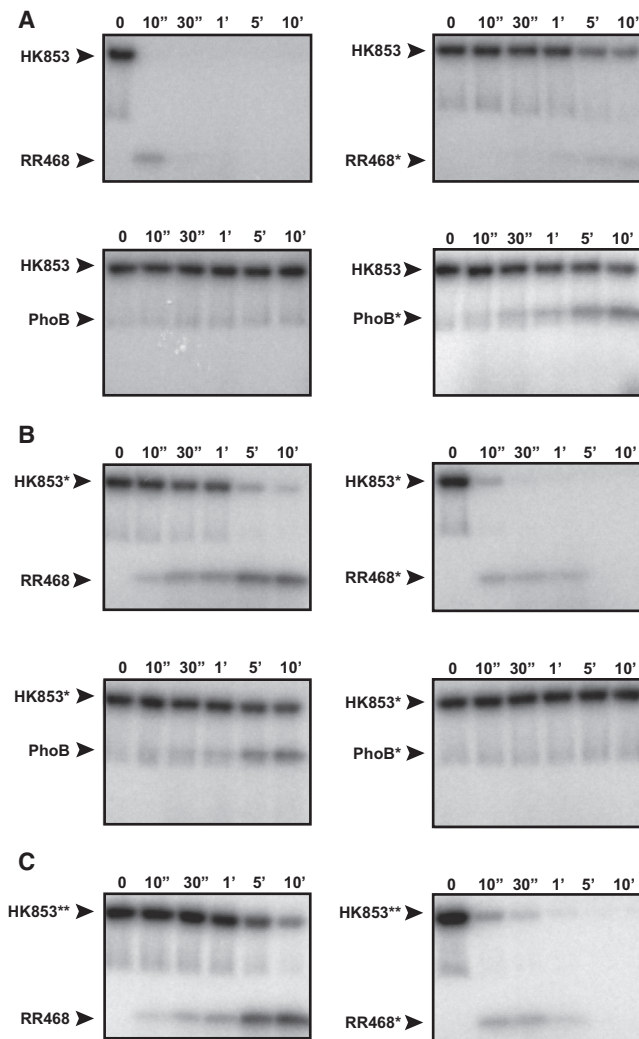


Figure 2. Rational Rewiring of Phosphotransfer Specificity

Phosphotransfer assays for wild-type and mutant two-component proteins. In each panel, the histidine kinase indicated was autophosphorylated with [32 P- γ] ATP and then incubated with the response regulator indicated at 4°C. Samples were taken at the time points indicated and phosphotransfer assessed by SDS-PAGE and phosphorimaging.

(A and B) Wild-type HK853 (A) and HK853* (B), which harbors the substitutions A268V, A271G, T275M, V294T, D297E, were tested for phosphotransfer to RR468, RR468*, PhoB, and PhoB*. RR468* contains the substitutions V13P, L14I, I17M, and N21V. PhoB* contains the substitutions P13V, I14L, M17I, and V21N.

(C) HK853**, which harbors the substitutions A268V, A271G, and T275M was tested for phosphotransfer to RR468 and RR468*.

See also Figures S2 and S3.

bifunctional with strong phosphatase activity for RR468~P (Casino et al., 2009), the combination of phosphotransfer and subsequent dephosphorylation of RR468 led to a loss of radiolabeled HK853 and RR468 within 15 s (Figure 1B). The rapid disappearance of phosphorylated HK853 resulted from phosphotransfer to the regulator, not simply dephosphorylation of HK853 through hydrolysis. When HK853 was incubated with RR468(D53A), which cannot be phosphorylated, the kinase re-

mained phosphorylated for extended periods of time (Casino et al., 2009) (Figure S2A). Like HK853, the histidine kinase PhoR rapidly phosphorylated its cognate partner, PhoB (Figure 1B). As the PhoR construct harbors only modest phosphatase activity for PhoB~P, continuous phosphotransfer resulted in the accumulation of phosphorylated PhoB over a 1 min time course. Finally, we examined phosphotransfer from HK853 and PhoR to the noncognate regulators PhoB and RR468, respectively. Neither HK853 nor PhoR phosphorylated the noncognate substrate (Figure 1C). The modest decrease in intensity of the HK853 band likely results from dephosphorylation, not phosphotransfer (Figure S1B). These experiments demonstrate that HK853-RR468 and PhoR-PhoB have different phosphotransfer specificities, consistent with their different specificity residues.

Rewiring the Specificity of HK853-RR468 to Match that of PhoR-PhoB

To rewire HK853-RR468, we substituted the specificity residues of HK853 and RR468 with those found in PhoR and PhoB, respectively, producing HK853* (A268V, A271G, T275M, V294T, D297E) and RR468* (V13P, L14I, I17M, N21V; Figure 1A). We also substituted the specificity residues of PhoB with those found in RR468, producing PhoB* (P13V, I14L, M17I, V21N). The substitutions introduced into HK853 did not significantly affect kinase autophosphorylation (Figure S2B). We then examined phosphotransfer from HK853 and HK853* to the response regulators RR468, RR468*, PhoB, and PhoB* (Figure 2; Figure S3A). Because phosphotransfer from HK853 to RR468 is so rapid at room temperature (Figure 1B), we performed these assays at 4°C to facilitate the comparison of relative phosphotransfer rates.

As before, HK853 rapidly phosphorylated and dephosphorylated RR468, with a complete loss of radiolabel within 30 s (Figure 2A). HK853 phosphorylated RR468* at an extremely slow rate, indicating that the substitutions introduced into RR468* disrupted the cognate interaction. As expected, wild-type HK853 did not transfer to the noncognate regulator PhoB under these reaction conditions, even after 10 min. However, HK853 was capable of phosphorylating PhoB*, indicating that the introduction of RR468-like specificity residues into PhoB was sufficient to promote phosphorylation by HK853 (Figure 2A).

For HK853*, we observed significantly reduced rates of phosphotransfer to RR468, indicating that changes to the specificity residues of HK853 had diminished the cognate pairing of HK853 and RR468 (Figure 2B). Strikingly, however, HK853* rapidly phosphorylated and dephosphorylated RR468*, indicating that the substitutions in RR468* restored a robust interaction with HK853*. Consistent with its new specificity residues, we found that HK853* could phosphorylate PhoB, but not PhoB* (Figure 2B).

We confirmed that HK853* has phosphatase activity toward RR468*, but not RR468, by using [32 P] acetyl-phosphate to radiolabel RR468*; subsequent addition of HK853* led to a rapid loss in radiolabel compared to buffer alone (Figure S2C). This result indicates that HK853* stimulates the dephosphorylation of RR468*.

A mutant of HK853, designated HK853**, harboring only three of the five specificity mutations (A268V, A271G, T275M) behaved similar to HK853*, suggesting that these three residues in the

Table 1. Crystallographic Data and Refinement Statistics

Processed Data	HK ^f *	RR ^f *	HK [*] -RR [*]	HK-RR [*]
Wavelength (Å)	0.92	0.87	0.98	0.87
Resolution (Å)	72.98–2.70 (2.85–2.70)	35.74–1.80 (1.88–1.79)	48.34–3.00 (3.16–3.00)	46.32–3.10 (3.27–3.10)
R _{merge} (%)	0.057 (0.337)	0.078 (0.279)	0.060 (0.389)	0.071 (0.401)
R _{pim} (%)	0.023 (0.13)	0.030 (0.107)	0.036 (0.226)	0.035 (0.198)
Mean I/σ (I)	21.0 (5.6)	19.7 (7.6)	15.0 (3.7)	17.9 (4.1)
No. of reflections (observed/unique)	60,367/8277 (8,550/1,162)	84,433/10,950 (11,971/1,566)	43,627/12,140 (6,406/1,750)	108,863/ 22,038 (15,794/3,160)
Completeness (%)	99.5 (99.2)	100.0 (100.0)	98.3 (98.9)	99.9 (100.0)
Redundancy	7.3 (7.4)	7.7 (7.6)	3.6 (3.7)	4.9 (5.0)
Space group	C222 ₁	I222	I222	C222 ₁
Cell dimensions (Å)	a = 81.96 b = 160.38 c = 43.89	a = 53.98 b = 58.06 c = 71.47	a = 75.71 b = 85.31 c = 185.59	a = 119.32 b = 143.93 c = 138.97
Refined Data				
R _{factor} (%)	0.236	0.186	0.209	0.202
R _{free} (%)	0.279	0.223	0.252	0.253
Asymmetric unit composition	1HK	1RR	1HK:1RR	2HK:2RR
No. of protein atoms	1890	976	2856	5842
No. of water molecules	44	91	13	13
No. of ligand/ion	1	5	4	14
Rmsd				
Bond deviation (Å)	0.009	0.008	0.005	0.004
Angle deviation (°)	1.3	1.3	1.0	0.9
Media B-Factor (Å²)				
Main chain	70.3	11.4	72.7	71.3
Side chain	71.2	13.5	75.2	73.2
All atoms	70.7	12.4	73.9	72.2
Ramachandran Map (%)				
Favored	96.88	99.15	94.89	96.81
Allowed	3.12	0.85	4.83	3.06
Disallowed region	0	0	0.28	0.14
PDB accession code	4JAU	4JA2	4JAS	4JAV

Values in parentheses correspond to data for the highest resolution shell.

$$R_{\text{merge}} = \frac{\sum hkl \sum i |I(hkl)_i - \langle I(hkl) \rangle|}{\sum hkl \sum i I(hkl)_i}$$

$$R_{\text{pim}} = \frac{\sum hkl \sqrt{1/(n-1)} \sum i |I(hkl)_i - \langle I(hkl) \rangle|}{\sum hkl \sum i I(hkl)_i}$$

$$R_{\text{factor}} = \frac{\sum |F_o| - |F_c|}{\sum |F_o|}$$

R_{free} is the R_{factor} calculated with 5%–7% of the total unique reflections chosen randomly and omitted from refinement.

middle of α1 were sufficient to rewire interaction specificity (Figure 2C). Collectively, these findings demonstrate that introduction of PhoR-like and PhoB-like substitutions into HK853 and RR468 was sufficient to reprogram their phosphotransfer specificity while maintaining phosphotransfer and dephosphorylation rates comparable to those seen in the wild-type proteins.

Structural Characterization of the Rewired Complex Reveals Changes in Relative Orientation between Interacting Proteins

To investigate the effects of the new specificity residues on partner recognition, we solved an X-ray crystal structure of the rewired complex formed by HK853* and RR468* (HK^{*}-RR^{*}; Table 1), which can engage in both phosphotransfer and phosphatase reactions (Figure 2B; Figure S2C). The rewired complex

preserves the stoichiometry of the original complex (HK-RR; Protein Data Bank [PDB] 3DGE; Casino et al., 2009): HK853* forms a homodimer that interacts with two molecules of RR468* (HK₂-2RR; Figure 3). In the rewired complex, the HK₂-2RR is generated by crystallographic 2-fold symmetry while in the HK-RR complex the asymmetric unit contained HK₂-2RR (Table 1). Further, the structures of the individual components are highly similar. The kinases superimpose with a root-mean-square deviation (rmsd) value of 1.82 Å (Table 2; Figure S4A). The superposition of individual domains shows even more similarity, with rmsd values of 1.0 Å and 0.87 Å for the DHP (residues 245–317) and CA (residues 320–480) domains, respectively. The slightly greater rmsd value for the kinases relative to individual domains results from a 19.7° rigid body rotation of the HK853* CA domain toward α1 of the DHP domain, which agrees with

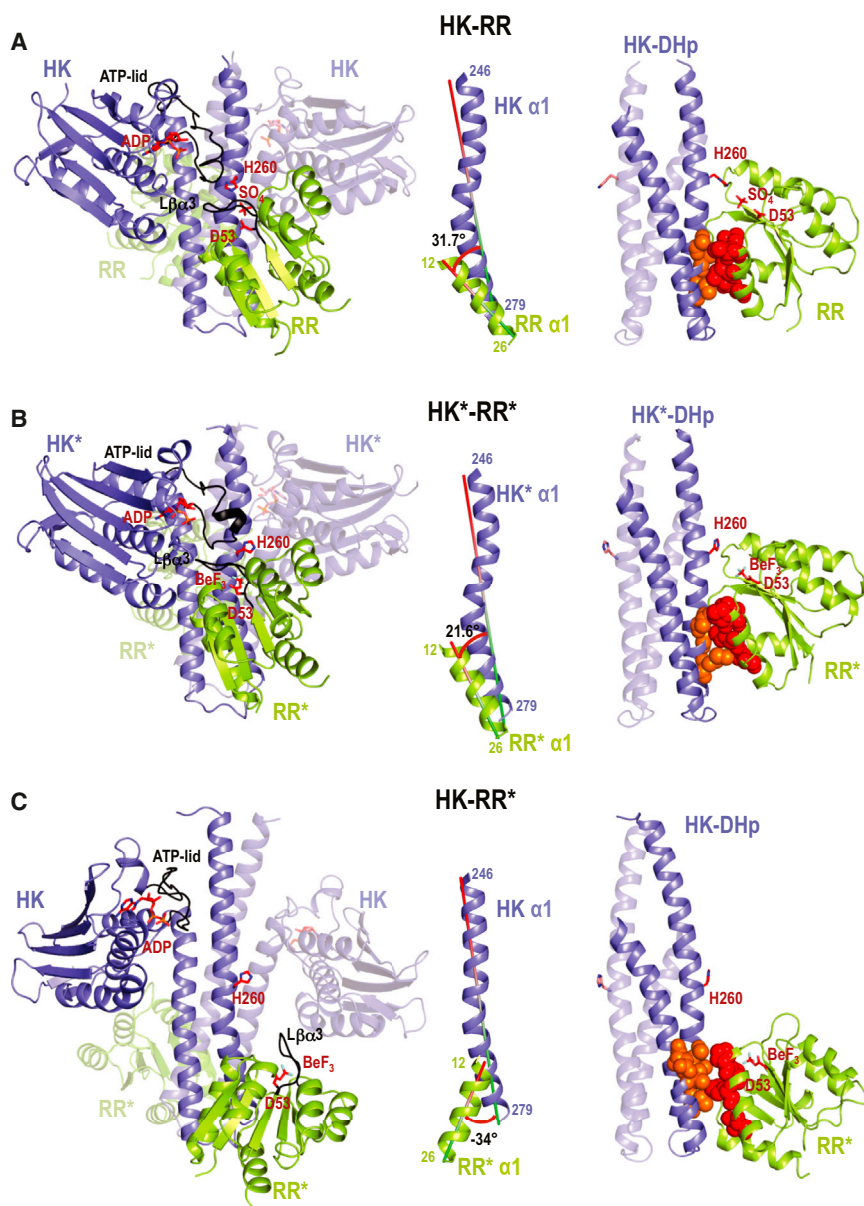


Figure 3. Crystal Structures of the Wild-Type Complex HK-RR, the Rewired and Functional HK*-RR* Complex, and the Impaired HK-RR* Complex

(A–C) Cartoon representations of HK-RR complex with HK853 bound to ADP and RR468 D53 bound to SO_4 (A), HK*-RR* complex with HK853* bound to ADP and RR468* D53 bound to BeF_3^- (B), and HK-RR* complex with HK853 bound to ADP and RR468* D53 bound to BeF_3^- (C). Left: cartoon representations of the overall structure of the three complexes formed by a homodimeric HK (blue with one subunit transparent) bound to two molecules of RR (yellow-green with one molecule transparent). In each complex, the ATP-lid in the HK and the $\beta 3$ - $\alpha 3$ linker in the RR are colored in black; the phosphorylatable residues H260 and D53 as well as bound ligands ADP, sulfate (SO_4), and beryllium trifluoride (BeF_3) are shown as sticks. Middle: the angle formed between the interacting helices HK $\alpha 1$ (246–279) and RR $\alpha 1$ (12–26) for each complex is shown. Right: HK-RR interface shown by the DHp domain (with one subunit transparent) bound to one RR with the critical specificity residues (13, 14, 17, and 21 in red for RR468; and 268, 271, 275, 294, and 297 in orange for HK853) highlighted in space-filling spheres. See also Figures S4–S6 and Table S1.

the structural plasticity and dynamic nature reported for the CA domain (Albanesi et al., 2009). RR468* has an almost identical structure to RR468 in the two functional complexes, HK-RR and HK*-RR*, with an rmsd of 0.6 Å (Table 3).

Despite high similarity at the domain level, the arrangement and relative orientation of the kinase with respect to the regulator differs in the rewired complex. In particular, RR468* is rotated 17.5° and translated 0.5 Å along the DHp domain, such that the angle between $\alpha 1$ of HK853* (residues 246–279) and $\alpha 1$ of RR468* (residues 12–26), the two key structural elements for complex formation, is 21.6° (Figure 3B). In the HK-RR complex, this same angle is 31.7° (Figure 3A). Because of this rotation, the HK853*-RR468* complex has a more parallel orientation between $\alpha 1$ in the regulator and the kinase helical bundle. In this orientation, RR468* loses some interactions with the DHp α -helix 2 and increases interactions with the CA domain. In particular,

RR468* in the HK*-RR* complex could acquire the disposition of RR468 in HK-RR without steric crystallographic clashes.

Although HK853 phosphorylates and dephosphorylates the mutant RR468* very slowly (Figure 2A; Figure S2C), we were able to solve a structure of these proteins in complex (HK-RR*). The asymmetric unit showed HK₂-2RR stoichiometry with almost 2-fold symmetry (Table 1), broken due to a slightly different relative disposition of the CA domain with respect to the DHp domain (~18.8°), confirming the previously mentioned plasticity of the CA domain (Figure S4C). Both HK subunits in the HK-RR* complex adopt a conformation that is more similar to the free form of HK853 (HKf; PDB: 2C2A; rmsd = 2.2 Å) than to the kinase in the HK-RR complex (rmsd = 5.6 Å; Table 2; Figure S4). The structure of RR468* in the HK-RR* complex is similar to RR468* in the HK*-RR* complex (rmsd = 0.6 Å, Table 3), but the RR468* molecule in HK-RR* adopts a totally different

Table 2. Rmsd Differences in the HK Component

Rmsd (Å)	HK-RR (3DGE) ^a	HK*-RR*	HK-RR*	HKf (2C2A) ^a	HKf*
HK-RR	–	1.82	5.6	5.2	4.95
HK*-RR*	–	–	4.8	4.35	4.1
HK-RR*	–	–	–	2.16	1.92
HKf	–	–	–	–	0.89

Residues 245–480.

^aPDB codes for the previously published structures.

position relative to the kinase. In the HK-RR* complex, RR468* α 1 is rotated $\sim 55^\circ$ and slightly displaced (~ 1.0 Å) relative to RR468* and RR468 in the rewired HK*-RR* and native HK-RR complexes, respectively (Figure 3C). Many of the intermolecular contacts seen in the productive HK-RR and HK*-RR* complexes are lost in the HK-RR* complex, consistent with its greatly diminished phosphotransfer rate (Table S1). Finally, the phosphorylatable residues in RR468* (Asp53) and HK853 (His260) are extremely far apart (19.0 Å) and improperly oriented for any catalytic reaction (Figure 3C).

Given the structural data for the functional complexes, HK-RR and HK*-RR*, we conclude that there is a permissible range of rotational motion of the kinase relative to the regulator that allows proper positioning of the active site while accommodating new interfacial residues.

The Active Center of the Rewired Complex Is a Snapshot of a New Intermediate State in Phosphotransfer

A closer view of the active sites in the HK*-RR* and HK-RR* complexes shows the phosphomimetic beryllium trifluoride (BeF_3^-) bound to the catalytic Asp53 of RR* in both cases. In HK*-RR*, the BeF_3^- is placed similarly to the sulfate found in the active site of the HK-RR complex, but the Be atom is slightly closer to the phosphorylatable His260 (Be-His260 $C\alpha = 7.85$ Å) than the sulfur atom of the sulfate in the HK-RR complex (S-His260 $C\alpha = 8.30$ Å; Figure 4). However, Met55 of RR468* is interposed between the His and the BeF_3^- in the HK*-RR* structure, forcing an alternative rotamer for His260 that points away from the active site. Thus, the structure of the HK*-RR* mutant complex may represent an earlier phase of the phosphatase reaction, when the phosphoryl group is still bound to the response regulator. Alternatively, if His260 acquired the rotamer conformation observed in the HK-RR complex, the distance between the phosphoacceptor nitrogen of this residue and the Be atom in the HK*-RR* complex would be 3.6 Å, a distance compatible with phosphotransfer (Figure 4). This observation suggests that the conformation captured in the crystal could, instead, correspond to the end of the phosphotransfer reaction just prior to complex dissociation. Because the phosphatase reaction is not the reverse of a phosphotransfer reaction (Hsing and Silhavy, 1997), the active center observed in the crystal could correspond to either of these reactions.

Introduction of New Specificity Residues Does Not Affect Global Structural Integrity

Structural differences between the different HK-RR complexes could be imposed by specific requirements for partner recognition or could reflect intrinsic changes in the individual proteins re-

Table 3. Rmsd Differences in the RR Component

Rmsd (Å)	HK-RR	HK*-RR*	HK-RR*	RRf*
HK-RR	–	0.61	0.69	0.67
HK*-RR*	–	–	0.6	0.54
HK-RR*	–	–	–	0.47

Residues 2–121.

sulting from the point mutations. To address this issue, we solved the structures of the free forms of HK853* (HKf*) bound to ADP and RR468* (RRf*) bound to BeF_3^- (Table 1). The conformations of HKf* and HKf are almost identical (rmsd = 0.9 Å for the superposition of the structures; Table 2; Figure S4B). However, there are local changes around the mutated residues that can be attributed to interactions between DHP α helices 1 and 2 mediated by the new side chains. In HKf* V268 and M275, together with T294 and F291 from α 2 and Y272 from α 1, generate a hydrophobic network (Figure 5A). These interactions induce changes in the exposed recognition surface and could impair interaction with the regulator. The flexibility of the new Met side chain seems to play a key role in this network because it is sandwiched between the Y272 and F291 aromatic rings (Figure 5A). The interaction of V268 and M275 with the complementary surface provided by the mutated residues of RR468* promotes the disappearance of this hydrophobic network in the productive complex (Figure 5B).

As with HK853*, comparison of RR468* in isolation and in the HK*-RR* complex shows minimal structural differences (Table 3) that are localized around the mutated residues. The I17M mutation seems to have the biggest structural impact on RR468* because the new Met side chain now mediates a hydrophobic interaction with F107 that was not present in RR468 (Figure 5C). This interaction involves a 2.4 Å displacement of F107 toward M17, a movement that brings the β 5- α 5 linker (L β α 5) closer to α 1. In the HK-RR complex, these two structural elements of RR468 clamp α 1 of the kinase's DHP domain. Although the M17-F107 interaction occurs in both RRf* and HK-RR*, F107 is positioned perpendicular to the M17 side chain in the HK*-RR* complex, suggesting that mutations in HK* may compensate for the presence of M17 (Figure 5C). The positioning of F107 in HK*-RR* is similar to that seen in HK-RR, suggesting this conformation may be important for the formation of a productive complex.

Systematic Mutational Characterization of the Rewired Interface

To further analyze the effects of individual substitutions at the HK853-RR468 interface (Figure 6A), we constructed all possible mutational intermediates separating the HK-RR and HK*-RR* pairings. Consistent with our previous finding that only three of the five mutations (A268V, A271G, and T275M) in HK853 are necessary to rewire the interface, residues V294 and D297 do not make interprotein contacts in the HK*-RR* structure (Table S1). We therefore constructed three single and three double mutants in HK853; along with the wild-type and triple mutant, there were eight different residue combinations for the kinase. For RR468, we made four single, six double, and four triple mutants; along with the wild-type and quadruple mutant (V13P, L14I, I17M,

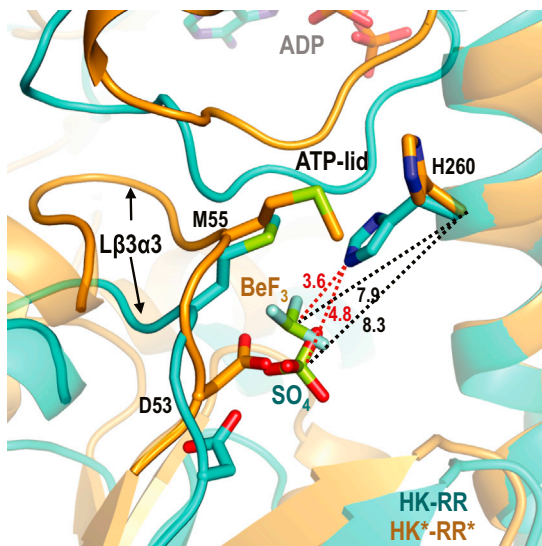


Figure 4. Comparison of the Active Center in the HK-RR and HK*-RR* Complexes

Close-up view of the active center with a superposition of HK-RR (in cyan) and HK*-RR* (in orange) in cartoon representation. The phosphorylatable residues H260 and D53, residue M55, and the bound ligands (sulfate [SO₄]) in the HK-RR complex and beryllium trifluoride (BeF₃) in the HK*-RR* complex are shown as sticks. Distances are shown by dashed lines; in black for C_α of H260 in HK-RR with the sulfur atom of SO₄ (8.3 Å) and for C_α of H260 in HK*-RR* with the Be atom of BeF₃ (7.9 Å); in red for εN of H260 in HK-RR with the sulfur atom of SO₄ (4.8 Å) and with the Be atom of BeF₃ (3.6 Å). See also Figures S4–S6 and Table S1.

and N21V), there was a total of 16 specificity residue combinations for the regulator. For simplicity, we refer to each of the mutants according to the identities of their specificity residues.

We systematically tested all 128 pairwise combinations of the eight kinases and 16 regulators for activity by incubating each autophosphorylated kinase with each regulator for 15 s (Figure 6B). Residue combinations that supported both phosphotransfer and dephosphorylation, such as the wild-type residues, led to a depletion of radiolabeled kinase with minimal accumulation of radiolabeled regulator. Combinations that supported only phosphotransfer led to an accumulation of phosphorylated regulator, and unproductive combinations retained phosphorylated kinase. Although the *in vivo* role of HK853/RR468 is unknown, studies with other two-component systems have demonstrated that both phosphotransfer and phosphatase activity are important for proper signal transduction (Huynh and Stewart, 2011). Therefore we identified functional kinase-regulator pairs for which (1) the intensity of the phosphorylated kinase band in the presence of regulator was less than 20% the intensity of the kinase band in the presence of buffer alone; and (2) the intensity of the phosphorylated regulator band was less than 10% the intensity of the autophosphorylated kinase band in the presence of buffer. Of the 128 combinations, 43 pairs satisfied these criteria (Figures 6B and 6C).

Our systematic mutagenesis shed light on the amino acid combinations permissible at this protein interface. For example, the profile of HK853 against the 16 regulator mutants demonstrates that robust phosphotransfer and dephosphorylation are

retained for all regulators except those harboring the I17M mutation (Figure 6B). For half of these pairings, the defect resulting from an I17M substitution can be rescued by the substitution A271G in the kinase. Given the similarity in size and nature between isoleucine and methionine, it is difficult to rationalize the strong impact of this mutation. However, our structural data indicated that the interaction of M17 with F107 could compromise proper packing of RR468* with HK853 DHP α1, thereby precluding a productive interaction (Figure 5C). Similarly, substituting a methionine residue into the kinase disrupted phosphatase activity, as evidenced by the inability of HK853(AAM), HK853(VAM), and HK853(AGM) to dephosphorylate the majority of regulator mutants (Figure 6B). In the HK*-RR* structure, the side chain of M275 lies within the hydrophobic pocket generated by RR468* residues M17, F20, and V21 (Figure 6A). A comparison with HK-RR shows that the residues M275 and M17 would have clashed if the displacement of RR468* α1 had not generated the hydrophobic pocket in HK*-RR*. In the new interface, the polar bond between T275 and N21 is replaced by a hydrophobic interaction between M275 and M17. This arrangement is further facilitated by the A271G mutation in HK* because the original alanine side chain would have clashed with M17 in RR*. Together, these findings illuminate the conformational restrictions imposed by individual residues that underlie amino acid coevolution, which in turn enabled the identification of specificity residues by statistical covariation analyses (Skerker et al., 2008).

Some combinations of residues yielded more promiscuous proteins. For instance, HK853(VGT) phosphorylated and dephosphorylated ten of the 16 regulators, including both the wild-type regulator and the quadruple mutant (Figure 6B). By comparison, wild-type HK853 phosphorylates and dephosphorylates eight of the regulators, including its partner RR468 but not the quadruple mutant. The flexibility introduced by glycine (A271G) may lead to productive interactions with many regulators. Conversely, some residue combinations interact with a very limited number of regulators. For instance, RR468(PLMV) interacted poorly with almost all kinase partners, and HK853(VAM) could phosphorylate and dephosphorylate only a single regulator.

Analysis of these mutational intermediates also demonstrated the interdependence of interface residues. The double mutant HK853(VAM) weakly phosphorylates each of the regulators, although its phosphatase activity is limited to RR468(PIIV; Figure 6B). However, either the A268V or the T275M mutation in HK853 by itself allows the kinase to strongly phosphorylate eight or six of the regulators, respectively. As another example, the mutation A268V has little effect on the wild-type kinase and its phosphotransfer profile looks essentially identical to the starting protein (Figure 6B). However, when introduced in the context of HK853(AGT), this mutation affects interactions with several of the mutant regulators. Thus, the effect of individual substitutions on specificity is highly context-dependent and difficult to predict from the behavior of the individual mutations.

Mutational Trajectories between the Wild-Type and Mutant Interfaces

Having a complete characterized set of mutational intermediates also sheds light on the evolution of two-component signaling protein specificity following duplication and divergence. There

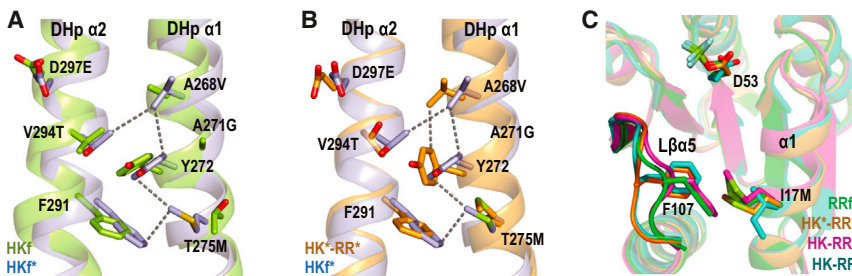


Figure 5. Differential Interactions in Free and Complex Structures

(A) DHp domains with a superposition of HKf (in green) and HKf* (in blue) to show new interactions resulting from the mutations introduced into HKf*: A268V, A271G, T275M, V294T, and D297E.

(B) DHp domains with a superposition of HKf* and HK853* from the HK*-RR* complex (in orange) to show changes in the interactions for M275.

(C) Superposition of RR468 in RRf* (green), HK-RR (cyan), HK*-RR* (orange), and HK-RR* (magenta) structures shows the interaction M17-

F107 and the different conformations of F107 and the $\beta 5$ - $\alpha 5$ linker in the RR alone or in complex. All the structures are shown in cartoon representation with the selected residues labeled in black and drawn as sticks.

See also Figures S4–S6 and Table S1.

are 5,040 possible mutational paths between two sequences that are seven letters long, assuming that only one amino acid is mutated at each step. Given our criteria for productive phosphotransfer and dephosphorylation (Figure 6C), we calculated that only 200 of these 5,040 possible paths, or 4%, retain functional kinase-regulator pairs along the entire path. Interestingly, two of the 43 kinase-substrate combinations that we deemed functional do not appear in any of the 200 mutational paths. For example, the pair HK853(AAM) and RR468(VILV) can be reached from a wild-type starting point, but all possible subsequent mutations produce a nonfunctional pair.

As noted above, the mutations T275M in the kinase and I17M in the regulator are often deleterious (Figure 6B). Consequently, these substitutions are often found along dead-end mutational paths. Of the 200 paths that maintain a productive interaction, 97 introduce T275M into the kinase as the final mutation, 64 paths introduce I17M into the regulator as the last mutation, and 29 paths end with the regulator mutation V13P. These patterns suggest that other mutations must be introduced first to effectively prime the interface for introduction of residues that restrict conformational freedom, such as methionine or proline. More generally, we infer that these residues contribute to specificity by eliminating interactions with noncognate regulators, rather than promoting interaction with the cognate regulator. For instance, HK853(VGT) phosphorylates and dephosphorylates ten of the 16 regulators; subsequent introduction of the T275M mutation eliminates interaction with seven of these ten regulators, but does not substantially improve interaction with the fully rewired, quadruple RR468 mutant (Figure 6B).

Although the majority of paths connecting the HK-RR and HK*-RR* pairs that maintain a functional interaction involve alternating mutations in the two proteins (Figure 6D), there are paths in which either the kinase or the regulator is completely changed through successive mutations while the other protein remains fixed. For instance, if the first three mutations produce RR468(PIIV) in any order, HK853 can then tolerate three successive mutations A268V followed by A271G/T275M in either order (Figure 6E). There are 12 mutational paths in which the kinase accumulates all of its mutations in succession. Similarly, if the first two mutations in a path yield the double mutant HK853(VGT), then the regulator, can accumulate four successive mutations, in seven different orders; there are 14 such paths in which the regulator accumulates all mutations in succession. In both of these examples, the protein that remains fixed while the other

protein accumulates substitutions is highly tolerant of mutations in its partner. RR468(PIIV) fully interacts with five of eight mutant kinases, and HK853(VGT) fully interacts with 10 out of the 16 mutant regulators (Figure 6B). Such tolerant intermediates may play important roles in the rewiring of two-component signaling interfaces that occurs during evolutionary processes such as duplication and divergence.

DISCUSSION

Despite the importance of protein-protein interaction specificity to the operation of cells, it remains relatively unclear how proteins use a finite set of amino acids to specifically recognize cognate partners. We addressed this question using two-component signaling proteins, which utilize a limited and known set of amino acids for partner recognition. The identification of these residues has guided the rational rewiring of two-component signaling pathways (Bell et al., 2010; Capra et al., 2010; Skerker et al., 2008), but a structural understanding of how rewiring is achieved was lacking. Here, we reprogrammed the structurally characterized complex *T. maritima* HK853-RR468 by introducing nine specificity residues from *E. coli* PhoR-PhoB. Although highly specific, phosphotransfer and dephosphorylation rates of PhoB-PhoR are slower than those of HK853-RR468. Strikingly, the introduction of PhoR-PhoB specificity residues did not impair the rapid reaction rates of HK853-RR468, despite the change in interaction specificity. This finding supports the notion that the specificity residues are required for recognition and proper positioning of the two partners, but other residues set the rates of the reactions (Pazy et al., 2009; Zapf et al., 1998).

The structure of the rewired complex HK*-RR* demonstrates that these functionally rewired two-component proteins preserve the overall structure of the wild-type complex along with catalytic activity. The kinase domains can reposition themselves slightly relative to each other and relative to the regulator to accommodate the foreign interfacial residues, but the overall complex retains wild-type character. Thus, rewiring leads primarily to local spatially restricted changes in the regions of each protein directly engaged in molecular docking.

Although the HK-RR and HK*-RR* complexes are similar, the HK-RR* complex harbors a completely different intermolecular orientation such that the phosphorylatable residues are no longer in proximity. We do not yet have a structure of the HK*-RR

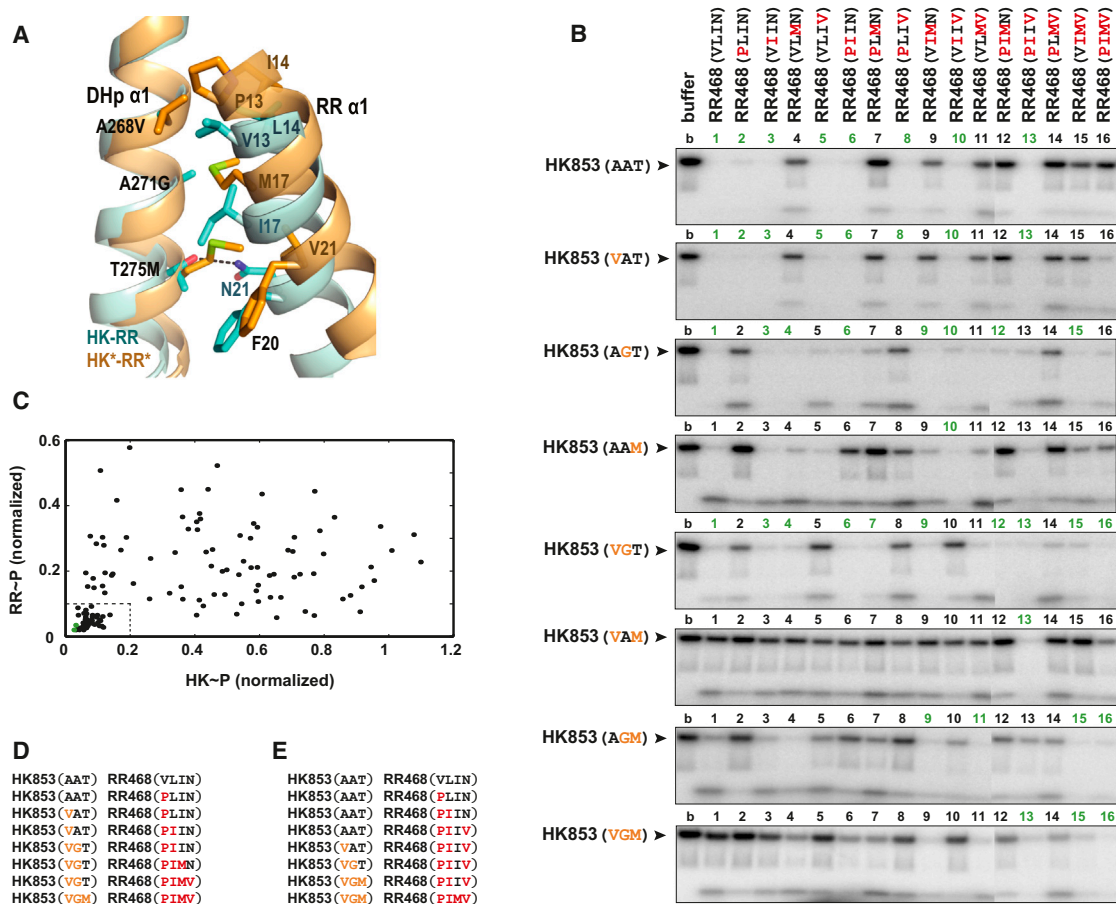


Figure 6. Phosphotransfer between All Possible Mutational Intermediates Separating HK-RR and HK*-RR*

(A) Superposition of HK-RR (in cyan) and HK*-RR* (in orange) complexes highlighting how mutations in DHp α 1 (A268V, A271G, and T275M) affect interactions with mutations in RR α 1 (V13P, L14I, I17M, and N21V) and F20. A dashed line represents a polar interaction between N21 and T275 in the HK-RR complex.

(B) Phosphotransfer assays for wild-type HK853 and HK853 harboring all possible combinations of one, two, or three PhoR-like specificity substitutions present in HK853** (A268V, A271G, and T275M). Each lane represents the incubation of the indicated autophosphorylated kinase with the indicated response regulator for 15 s at room temperature. Reactions 1–11 and 12–16 were run on separate SDS-PAGE gels; the resulting phosphorimages were contrasted identically and stitched together.

(C) The HK and RR bands from the phosphotransfer experiments in (B) were quantified and plotted. For each mutational pairing, the x-axis value indicates the intensity of the autophosphorylated HK band (HK~P) and the y-axis value indicates the intensity of the phosphorylated response regulator band (RR~P). In each case, band intensities were normalized to the intensity of the autophosphorylated kinase incubated without RR (lane 1 of each gel in B). Green points indicate the pairs HK853-RR468 and HK853*-RR468*. The box in the lower left indicates pairings deemed functional; a low level of both the kinase and regulator bands reflects efficient phosphotransfer and dephosphorylation. The 43 functional pairings are indicated in green in (B).

(D) One example of a mutational path from the wild-type to the rewired complex in which each intermediate state is functional.

(E) An example of a mutational path in which all mutations to the kinase occur in three successive steps.

See also Figures S4–S6 and Table S1.

complex, which can participate in slow phosphotransfer but not dephosphorylation. Because HK853* is competent as a phosphatase for other partners, the lack of activity with respect to RR is probably due to a mismatch at the interaction interface, which could force the regulator to dock in the wrong orientation. Alternatively, the regulator may bind at the correct position but too weakly to support rapid phosphotransfer and dephosphorylation.

How do individual residues contribute to specificity? In some cases, disruptive mutations that change the size or nature of a residue can be restored by balancing mutations at neighboring inter- or intramolecular positions. This sort of intermolecular

compensation is consistent with the extensive amino acid coevolution previously documented for two-component signaling proteins (Skerker et al., 2008). However, it is difficult to ascribe a role to individual specificity residues, as the effect of a given substitution can be highly context-dependent. In general, our systematic mutagenesis study indicated that individual residues do not typically contribute equally or additively to specificity. This interdependence of specificity residues resonates with other recent studies suggesting that amino acid epistasis in proteins is extensive and common (Breen et al., 2012; Levin et al., 2009; Ortlund et al., 2007).

Our work also has implications for understanding the evolutionary processes of duplication and divergence, which underlie the massive expansion of two-component signaling protein families in bacteria (Capra and Laub, 2012; Capra et al., 2012). After duplication, paralogous signaling proteins must become insulated with respect to phosphotransfer while retaining an interaction with their cognate partners. Examples of the mutational trajectories that proteins follow, and any constraints they face, are largely unknown. Although *T. maritima* HK853-RR468 and *E. coli* PhoR-PhoB are not closely related, our systematic analysis of mutational trajectories between them provides insights into how specificity evolves. Our finding that only 4% of the theoretically possible evolutionary paths retain a functional interaction suggests that trajectories through sequence space may be severely constrained. Previous work on mutational trajectories that convert β -lactamase from a drug-sensitive to drug-resistant state also found strong constraints with only eight of 120, or 6%, of paths permissible (Weinreich et al., 2006).

None of the mutational combinations we tested were fully insulated from both the starting HK-RR and the final HK*-RR* complex, i.e., none forms an orthogonal interacting pair. This finding highlights the potential evolutionary importance of promiscuous states of the binding interface (Aharoni et al., 2005; Matsumura and Ellington, 2001). We speculate that ancestral two-component proteins may have harbored such promiscuity; following duplication and divergence, the paralogs could have gained specificity simply through the accumulation of mutations that disrupt a subset of interactions seen in the ancestral state. This process of subfunctionalization represents a rapid route to specificity and could help explain the apparent ease with which paralogous protein families have expanded.

Our results also have implications for protein design efforts. As noted, there are dependencies between neighboring residues on one molecule, and between residues on two different protein partners. Thus, the HK853-RR468 interface can tolerate certain substitutions only in combination—an effect not easily predicted based on a consideration of how the individual substitutions behave. Consequently, efforts to design or engineer novel protein-protein interfaces will have to tackle this combinatorial problem. Our findings also underline the importance of subtle backbone flexibility in protein design (Humphris and Kortemme, 2008; Smith and Kortemme, 2008) because a static complex would not properly accommodate the introduction of a new set of specificity residues. In sum, our studies have provided important insights into the molecular and structural basis of two-component signaling specificity and also highlight the significant challenges that remain in computationally predicting (Chen and Keating, 2012) the effects of mutations and in designing interfaces de novo.

EXPERIMENTAL PROCEDURES

Cloning, Mutagenesis, and Protein Purification

All site-directed mutagenesis (see Table S2 for primers) was done with Gateway (Invitrogen) cloning vectors as described previously (Skerker et al., 2008). Mutagenized and sequence-verified protein sequences were moved from pENTR vectors into pDEST vectors using the Gateway LR reaction (pDEST-His₆-MBP for HK853 and PhoR; pDEST-His₆-TRX for PhoB; pDEST-His₆ for RR468). For crystallization assays, the complete cytoplasmic portion of HK853* (232–489) was recloned from pDEST-His₆-MBP into pET24b and

full-length RR468* (1–122) was recloned from pDEST-His₆ into pET22b, using in both cases, the In-Fusion HD cloning technology (Clontech; Table S3). Expression and purification was carried out as described previously (Casino et al., 2009; Skerker et al., 2005).

Phosphotransfer Assays

Autophosphorylation and phosphotransfer assays were performed as described previously (Capra et al., 2010). Histidine kinases diluted to 5 μ M in HKEDG buffer (10 mM HEPES-KOH pH 8.0, 50 mM KCl, 10% glycerol, 0.1 mM EDTA, 2 mM dithiothreitol) supplemented with 5 mM MgCl₂ were autophosphorylated with 500 μ M ATP and 0.5 μ Ci [γ -³²P]-ATP (from a stock at ~6,000 Ci/mmol, Perkin Elmer). PhoR was autophosphorylated for 1 hr at 30°C; HK853 and all HK853 mutants were autophosphorylated for 20 min at room temperature (see Figure S2B for autophosphorylation time course). The autophosphorylated kinase mixture was added directly to response regulator (at 5 μ M in HKEDG buffer supplemented with 5 mM MgCl₂). Reactions were quenched with 4 \times loading buffer (500 mM Tris-HCl pH 6.8, 8% SDS, 40% glycerol, 400 mM β -mercaptoethanol) and analyzed by SDS-PAGE and phosphorimaging. For reactions carried out at 4°C, the autophosphorylated histidine kinase was incubated at 4°C for 5 min prior to addition of chilled response regulator. Radiolabeled bands were quantified with Imaged software.

Phosphatase Assays

To perform the phosphatase assays in Figure S2C, [³²P]acetyl-phosphate was freshly synthesized as described previously (Jagadeesan et al., 2009). RR468 (at 10 μ M in HKEDG buffer supplemented with 5 mM MgCl₂) was mixed 1:1 with [³²P]acetyl-phosphate and incubated for 1 hr at room temperature. The mixture was washed three times with cold HKEDG buffer and the concentration of MgCl₂ subsequently adjusted to 5 mM. The phosphorylated regulator was chilled at 4°C for 5 min and then incubated with buffer or with an equimolar amount of kinase (both prechilled) for the times indicated. Because RR468* autophosphorylates more poorly than RR468 using this method, both regulator and kinase concentrations were doubled to 20 μ M starting concentration to measure RR468*~P dephosphorylation.

Crystallization, Data Collection, and Model Building

Crystallization of HKf* and RRf* proteins, HK*-RR* and HK-RR* complexes was achieved by the vapor diffusion method, using the sitting drop technique, mixing 0.6 μ l of protein and 0.6 μ l of reservoir solution. Crystals of HKf* were obtained in 8% PEG4000, 0.8 M LiCl, and Tris pH 8.5 by mixing 10 mg/ml of protein, 4 mM ADP, and 4 mM MgCl₂. Crystals of RRf* in complex with BeF₃⁻ were obtained in 50% PEG400, NaAc pH 4.6, and 0.2 M Li₂(SO₄) mixing 15 mg/ml of protein, 30 mM NaF, 5 mM BeSO₄, and 7 mM MgCl₂. Crystals of the complexes HK*-RR* and HK-RR* were obtained in 2.2 M (NH₄)₂SO₄ and Bis-Tris pH 5.5 by cocrystallization mixing 10 mg/ml of HK853* or HK853, 7.5 mg/ml of RR468*, 4 mM ADP, 30 mM NaF, 5 mM BeSO₄, and 7 mM MgCl₂. Crystals of HKf* were cryoprotected by increasing PEG4000 to 16% and by the addition of 20% sucrose while crystals of the complexes were cryoprotected by addition of 35% sucrose. X-ray diffraction data were collected at Diamond Light Source I04-1 (Oxfordshire, UK) for HKf*, at European Synchrotron Facility ID23-2 (ESRF, Grenoble, France) for RRf*, and at ESRF ID23-1 and ID23-2 for the complexes HK*-RR* and HK-RR*, respectively. Data reduction was performed using XDS, Pointless, and Scala to a Bragg space of 2.7 Å for HKf*, 1.8 Å for RRf*, 3.0 Å for HK*-RR* complex, and 3.1 Å for HK-RR* complex. Phases were obtained by molecular replacement using Phaser and the final models were obtained by subsequent cycles of refinement with Refmac5 and model building with the program Coot (Emsley and Cowtan, 2004). Despite the limited resolution for the complexes, the quality of the maps (Figure S6) allowed model building and unambiguous side chain assignments except for the first and last residues in HK* (232–243; 481–490) and HK (chain A 232–233; 480–490 and chain B 232–235; 480–490) where electronic density was absent, which reflects the elevated flexibility of these regions. Crystallographic data and refinement statistics are presented in Table 1. The programs Pointless, Scala, Phaser, and Refmac are contained in CCP4 Suite. Figures 3, 4, 5, and S4–S6 were produced using PyMOL (<http://www.pymol.org>). Superimpositions were carried out with Superpose from CCP4 Suite. Movement analysis was performed using the program Dyndom (Lee et al., 2003). In the

HK-RR and HK-RR* complexes, where the asymmetric unit is formed by HK₂-2RR, HK chain A and RR chain C were chosen for the structural comparisons. PDB accession codes for additional structures analyzed in the manuscript are 2C2A for HKf and 3DGE for HK-RR.

ACCESSION NUMBERS

The Protein Data Bank accession numbers for the 3D structures reported in this paper are 4JAU for HKf*, 4JA2 for RRF*, 4JAS for HK*-RR*, and 4JAV for HK-RR*.

SUPPLEMENTAL INFORMATION

Supplemental Information includes Supplemental Experimental Procedures, six figures, and three tables and can be found with this article online at <http://dx.doi.org/10.1016/j.str.2013.07.005>.

ACKNOWLEDGMENTS

We thank A. Keating and members of the Laub laboratory for helpful comments on the manuscript. We acknowledge the European Synchrotron Radiation Facility (ESRF) and Diamond Light Source (DLS) for provision of synchrotron radiation facilities, and we would like to thank ID23-1, ID23-2 (ESRF), and I04-1 (DLS) beamlines staff for assistance during data collection. M.T.L. is an Early Career Scientist at the Howard Hughes Medical Institute. This work was supported by an NSF CAREER award (MCB-0844442) to M.T.L., grants BIO2010-15424 from the Ministerio de Ciencia e Innovación and ACOMP2013/031 from Generalitat Valenciana to A.M., and NSF Graduate Research Fellowship to A.I.P. P.C. is recipient of a postdoctoral junior grant “Juan de la Cierva” from the Ministry of Economy and Competitiveness. The research leading to these results has received funding from the European Community's Seventh Framework Programme (FP7/2007-2013) under BioStruct-X (grant agreement number 283570).

Received: April 7, 2013

Revised: June 25, 2013

Accepted: July 3, 2013

Published: August 15, 2013

REFERENCES

- Aharoni, A., Gaidukov, L., Khersonsky, O., McQ Gould, S., Roodveldt, C., Tawfik, D.S., and Tawfik, D.S. (2005). The ‘evolvability’ of promiscuous protein functions. *Nat. Genet.* **37**, 73–76.
- Albanesi, D., Martín, M., Trajtenberg, F., Mansilla, M.C., Haouz, A., Alzari, P.M., de Mendoza, D., and Buschiazzo, A. (2009). Structural plasticity and catalysis regulation of a thermosensor histidine kinase. *Proc. Natl. Acad. Sci. USA* **106**, 16185–16190.
- Alm, E., Huang, K., and Arkin, A. (2006). The evolution of two-component systems in bacteria reveals different strategies for niche adaptation. *PLoS Comput. Biol.* **2**, e143.
- Ashenberg, O., Keating, A.E., and Laub, M.T. (2013). Helix bundle loops determine whether histidine kinases autophosphorylate in *cis* or in *trans*. *J. Mol. Biol.* **425**, 1198–1209.
- Bell, C.H., Porter, S.L., Strawson, A., Stuart, D.I., and Armitage, J.P. (2010). Using structural information to change the phosphotransfer specificity of a two-component chemotaxis signalling complex. *PLoS Biol.* **8**, e1000306.
- Breen, M.S., Kemena, C., Vlasov, P.K., Notredame, C., and Kondrashov, F.A. (2012). Epistasis as the primary factor in molecular evolution. *Nature* **490**, 535–538.
- Capra, E.J., and Laub, M.T. (2012). Evolution of two-component signal transduction systems. *Annu. Rev. Microbiol.* **66**, 325–347.
- Capra, E.J., Perchuk, B.S., Lubin, E.A., Ashenberg, O., Skerker, J.M., and Laub, M.T. (2010). Systematic dissection and trajectory-scanning mutagenesis of the molecular interface that ensures specificity of two-component signaling pathways. *PLoS Genet.* **6**, e1001220.
- Capra, E.J., Perchuk, B.S., Skerker, J.M., and Laub, M.T. (2012). Adaptive mutations that prevent crosstalk enable the expansion of paralogous signaling protein families. *Cell* **150**, 222–232.
- Casino, P., Rubio, V., and Marina, A. (2009). Structural insight into partner specificity and phosphoryl transfer in two-component signal transduction. *Cell* **139**, 325–336.
- Casino, P., Rubio, V., and Marina, A. (2010). The mechanism of signal transduction by two-component systems. *Curr. Opin. Struct. Biol.* **20**, 763–771.
- Chen, T.S., and Keating, A.E. (2012). Designing specific protein-protein interactions using computation, experimental library screening, or integrated methods. *Protein Sci.* **21**, 949–963.
- Codoñer, F.M., and Fares, M.A. (2008). Why should we care about molecular coevolution? *Evol. Bioinform. Online* **4**, 29–38.
- Emsley, P., and Cowtan, K. (2004). Coot: model-building tools for molecular graphics. *Acta Crystallogr. D Biol. Crystallogr.* **60**, 2126–2132.
- Fisher, S.L., Kim, S.K., Wanner, B.L., and Walsh, C.T. (1996). Kinetic comparison of the specificity of the vancomycin resistance VanS for two response regulators, VanR and PhoB. *Biochemistry* **35**, 4732–4740.
- Galperin, M.Y. (2005). A census of membrane-bound and intracellular signal transduction proteins in bacteria: bacterial IQ, extroverts and introverts. *BMC Microbiol.* **5**, 35.
- Gao, R., and Stock, A.M. (2009). Biological insights from structures of two-component proteins. *Annu. Rev. Microbiol.* **63**, 133–154.
- Hsing, W., and Silhavy, T.J. (1997). Function of conserved histidine-243 in phosphatase activity of EnvZ, the sensor for porin osmoregulation in *Escherichia coli*. *J. Bacteriol.* **179**, 3729–3735.
- Humphris, E.L., and Kortemme, T. (2008). Prediction of protein-protein interface sequence diversity using flexible backbone computational protein design. *Structure* **16**, 1777–1788.
- Huynh, T.N., and Stewart, V. (2011). Negative control in two-component signal transduction by transmitter phosphatase activity. *Mol. Microbiol.* **82**, 275–286.
- Igo, M.M., Ninfa, A.J., Stock, J.B., and Silhavy, T.J. (1989). Phosphorylation and dephosphorylation of a bacterial transcriptional activator by a transmembrane receptor. *Genes Dev.* **3**, 1725–1734.
- Jagadeesan, S., Mann, P., Schink, C.W., and Higgs, P.I. (2009). A novel “four-component” two-component signal transduction mechanism regulates developmental progression in *Myxococcus xanthus*. *J. Biol. Chem.* **284**, 21435–21445.
- Keskin, O., Gursoy, A., Ma, B., and Nussinov, R. (2008). Principles of protein-protein interactions: what are the preferred ways for proteins to interact? *Chem. Rev.* **108**, 1225–1244.
- Laub, M.T., and Goulian, M. (2007). Specificity in two-component signal transduction pathways. *Annu. Rev. Genet.* **41**, 121–145.
- Lee, R.A., Razaz, M., and Hayward, S. (2003). The DynDom database of protein domain motions. *Bioinformatics* **19**, 1290–1291.
- Levin, K.B., Dym, O., Albeck, S., Magdassi, S., Keeble, A.H., Kleanthous, C., and Tawfik, D.S. (2009). Following evolutionary paths to protein-protein interactions with high affinity and selectivity. *Nat. Struct. Mol. Biol.* **16**, 1049–1055.
- Matsumura, I., and Ellington, A.D. (2001). In vitro evolution of beta-glucuronidase into a beta-galactosidase proceeds through non-specific intermediates. *J. Mol. Biol.* **305**, 331–339.
- Ortlund, E.A., Bridgman, J.T., Redinbo, M.R., and Thornton, J.W. (2007). Crystal structure of an ancient protein: evolution by conformational epistasis. *Science* **317**, 1544–1548.
- Pazy, Y., Wollish, A.C., Thomas, S.A., Miller, P.J., Collins, E.J., Bourret, R.B., and Silversmith, R.E. (2009). Matching biochemical reaction kinetics to the timescales of life: structural determinants that influence the autodephosphorylation rate of response regulator proteins. *J. Mol. Biol.* **392**, 1205–1220.
- Skerker, J.M., Prasol, M.S., Perchuk, B.S., Biondi, E.G., and Laub, M.T. (2005). Two-component signal transduction pathways regulating growth and cell cycle progression in a bacterium: a system-level analysis. *PLoS Biol.* **3**, e334.

Skerker, J.M., Perchuk, B.S., Siryaporn, A., Lubin, E.A., Ashenberg, O., Goulian, M., and Laub, M.T. (2008). Rewiring the specificity of two-component signal transduction systems. *Cell* 133, 1043–1054.

Smith, C.A., and Kortemme, T. (2008). Backrub-like backbone simulation recapitulates natural protein conformational variability and improves mutant side-chain prediction. *J. Mol. Biol.* 380, 742–756.

Stock, A.M., Robinson, V.L., and Goudreau, P.N. (2000). Two-component signal transduction. *Annu. Rev. Biochem.* 69, 183–215.

Weinreich, D.M., Delaney, N.F., Depristo, M.A., and Hartl, D.L. (2006). Darwinian evolution can follow only very few mutational paths to fitter proteins. *Science* 312, 111–114.

Zapf, J., Madhusudan, M., Grimshaw, C.E., Hoch, J.A., Varughese, K.I., and Whiteley, J.M. (1998). A source of response regulator autophosphatase activity: the critical role of a residue adjacent to the Spo0F autophosphorylation active site. *Biochemistry* 37, 7725–7732.